Nanomedicine: Nanotechnology, Biology, and Medicine
14 (2018) 2259–2270

nanomedjournal.com

Endoscopic molecular imaging of early gastric cancer using fluorescently labeled human H-ferritin nanoparticle

Yang Du, PhD[a,b,c,1], Kelong Fan, PhD[d,1], Hejun Zhang, MSc[e,1], Li Li, MSc[a], Peixia Wang, MSc[c,d], Jiuyang He, BS[c,d], Shigang Ding, MD[e,*], Xiyun Yan, PhD[c,d,**], Jie Tian, PhD[a,b,c,***]

[a]*CAS Key Laboratory of Molecular Imaging, The State Key Laboratory of Management and Control for Complex Systems, Institute of Automation, Chinese Academy of Sciences, Beijing, China*

[b]*Beijing Key Laboratory of Molecular Imaging, Beijing, China*

[c]*The University of Chinese Academy of Sciences, Beijing, China*

[d]*Key Laboratory of Protein and Peptide Pharmaceutical, Institute of Biophysics, Chinese Academy of Sciences, Beijing, China*

[e]*Department of Gastroenterology, Beijing Key Laboratory for Helicobacter Pylori Infection and Upper Gastrointestinal Diseases, Peking University Third Hospital, Beijing, China*

Received 13 January 2018; accepted 15 July 2018

Abstract

Optical imaging technologies improve clinical diagnostic accuracy of early gastric cancer (EGC). However, there was a lack of imaging agents exhibiting molecular specificity for EGCs. Here, we employed the dye labeled human heavy-chain ferritin (HFn) as imaging nanoprobe, which recognizes tumor biomarker transferrin receptor 1 (TfR1), to enable specific EGC imaging using confocal laser endomicroscopy (CLE). TfR1 expression was initially examined *in vitro* in gastric tumor cells and *in vivo* through whole-body fluorescence and CLE imaging in tumor-bearing mice. Subsequently, dye labeled HFn was topically applied to resected human tissues for EGC detection. CLE analysis of TfR1-targeted fluorescence imaging allowed distinction of neoplastic from non-neoplastic tissues ($P < 0.0001$), and TfR1 expression level was found to correlate with EGC differentiation degrees ($P < 0.0001$). Notably, the CLE evaluation correlated well with the immunohistochemical findings (κ-coefficient: 0.8023). Our HFn-nanoprobe-based CLE increases the accuracy of EGC detection and enables visualization of tumor margins and endoscopic resection.

Key words: Early gastric cancer; Confocal laser endomicroscopy; Human H-ferritin; Molecular imaging; Fluorescently labeled nanoprobe

Abbreviations: CLE, confocal laser endomicroscopy; EGC, early gastric cancer; HFn, human heavy-chain ferritin; TfR1, transferrin receptor 1; IHC, immunohistochemistry; FMI, Fluorescence molecular imaging; H&E, Hematoxylin and eosin; pCLE, probe-based confocal laser endomicroscopy; cryo-TEM, cryo-transmission electron microscopy; M-HFn, magneto-HFn nanoparticle.

Statement of Conflicts of Interest: The authors declare no potential conflicts of interest. All authors approved the publication of this manuscript.

Funding Support: Ministry of Science and Technology of China (2016YFA0201404, 2017YFA0205200); National Natural Science Foundation of China (81470083, 81527805, 81571810, 61231004, 81201186, 31530026 and 81671810); Research and Development Program of China (973) (2015CB755500); Young Elite Scientist Sponsorship Program by CAST (2015QNRC001); the Strategic Priority Research Program from Chinese Academy of Sciences (XDB02060010, XDA09030306); Key Research Program of Frontier Sciences, CAS (QYZDB-SSW-SMC013).

*Corresponding author at: Department of Gastroenterology, Peking 3rd Hospital, Beijing, China.

**Correspondence to: X. Yan, Key Laboratory of Protein and Peptide Pharmaceutical, Institute of Biophysics, Chinese Academy of Sciences, Beijing.

***Correspondence to: J. Tian, CAS Key Laboratory of Molecular Imaging of Chinese Academy of Sciences, Institute of Automation, Chinese Academy of Sciences, Beijing 100190, China.

E-mail addresses: dingshigang222@163.com (S. Ding), yanxy@sun5.ibp.ac.cn (X. Yan), jie.tian@ia.ac.cn. (J. Tian).

[1] These authors contributed equally to this paper.

https://doi.org/10.1016/j.nano.2018.07.007
1549-9634/

Almost 990,000 cases of gastric cancer are detected annually, and it is the second leading cause of cancer-related deaths worldwide due to the late detection.[1] Thus, early detection of gastric cancers through endoscopy provides an opportunity for intervention before the disease progresses to an advanced stage. Confocal laser endomicroscopy (CLE) is a recently developed optical imaging technique that is used to examine the gastrointestinal mucosa at the microscopic level, and CLE enables direct histological observation of the tissue *in vivo* by providing real-time, high-resolution, and high-magnification images.[2] Based on its diagnostic accuracy in gastric neoplasia detection, CLE is expected to be used in several potential applications, including in decreasing the requirement for repeated biopsies and determining the margins of gastric neoplasias before endoscopic resection.

A potentially powerful approach for facilitating endoscopic cancer detection and resection is the combined use of optical imaging technologies and tumor-targeted imaging agents.[3,4] White-light endoscopy is the primary method used to visualize and resect cancers of gastrointestinal tracts. However, white-light endoscopy presents several recognized shortcomings, including incomplete detection of multifocal and flat tumor boundaries, as well as inadequate visualization of tumor boundaries, which affects the thoroughness of resection. CLE has recently been widely used through combining with fluorescently labeled antibodies or peptides.[5–8] The CLE-enabled visualization of specific molecular targets provides a dynamic intravital imaging of larger tissues than conventional immunohistochemistry (IHC). However, no specific biomarker has been developed thus far for early gastric cancer (EGC) detection through targeted molecular imaging, and a high demand exists for the identification of new biomarkers for EGC detection.

Transferrin receptor 1 (TfR1), a transmembrane homodimeric glycoprotein, is an essential component in cell growth and iron-requiring metabolic processes. TfR1 has been found to be overexpressed in diverse cancers,[9] but TfR1 expression in gastric cancer and its correlation with the clinicopathologic parameters in EGCs remain unexplored. Currently, most TfR1-targeted strategies involve using the TfR1 ligand transferrin (Tf) or anti-TfR1 antibodies, but a limiting factor in both Tf- and antibody-based strategies is that TfR1 is also expressed at low levels in certain nontumor cells, and thus neither Tf nor anti-TfR1 antibodies distinguish these nontumor cells from tumor cells very well.[9] Intriguingly, TfR1 was recently identified as a human H-ferritin (HFn) receptor.[10] Ferritin is a spherical iron-storage protein composed of a self-assembled 24-subunit protein shell featuring an outer diameter of 12 nm and interior-cavity diameter of 8 nm, which accommodates up to 4500 Fe (III) atoms as an iron mineral core.[11,12] Because of this unique architecture, ferritin nanoparticles provide an optimal multifunctional nanoplatform.[13] Recently, a novel biomimetically synthesized magneto-HFn nanoparticle (M-HFn) was developed through encapsulating iron oxide nanoparticles inside a HFn shell, which binds to tumor cells with TfR1 overexpression. The catalysis of the oxidation of peroxidase substrates by the iron oxide core in the presence of hydrogen peroxide can produce a color reaction that is used for the visualization of tumor tissues. It was applied in the screening of 474 clinical specimens from patients with 9 types of cancers, and the results demonstrated that M-HFn distinguishes cancerous cells from noncancerous cells with high sensitivity (98%) and specificity (95%).[14] This work indicated that HFn nanoprobe presents a universal potential for cancer cell detection. More recently, HFn nanoprobes were found to be preferentially incorporated by TfR1-positive cells in a threshold-dependent manner.[15,16] This led us to hypothesize that HFn serves as a viable probe for molecular imaging of EGCs.

Here, we sought to develop a targeted-imaging strategy to enhance EGC detection using fluorescently labeled HFn nanoparticle in combination with clinical-grade CLE imaging, which enables enhanced differentiation between gastric tumor tissues and adjacent noncancerous tissues. The feasibility of the method was examined on the tumor-bearing mice, and also on the excised human EGC specimens (Figure 1). Given that endomicroscopy with the probe fluorescein is already in clinical use, *in vivo* molecular imaging in patients becomes feasible in the near future, and thus EGC diagnosis is potentially achieved by targeting TfR1.

Methods

Probe synthesis and characterization

Human HFn was produced and purified as described in our previous reports[14,15,17]; please see *SI Materials and Methods* for details related to probe synthesis/characterization.

Gastric tumor cell culture

The gastric tumor cell lines SGC-7901 and BGC-823, the normal human gastric epithelial cell line GES-1, and the TfR1-negative human breast cancer cell line MX-1 were purchased from American Type Culture Collection (ATCC). The cells were cultured in RPMI-1640 (Invitrogen) with 10% fetal bovine serum (Invitrogen) and 1% antibiotics at 37 °C under 5% CO_2.

Gastric tumor-bearing mice

Two gastric tumor-bearing mouse models (SGC-7901 and BGC-823) and TfR-1 negative MX-1 tumor bearing mouse model were established. SGC-7901, BGC-823 and MX-1 cells (1×10^6) in 1× PBS were transplanted subcutaneously in the backs of 5-week-old female Balb/c mice (Department of Experimental Animals, Peking University Health Science Center, Beijing, China). The experimental protocols were approved by the Institutional Animal Care and Use Committee at Peking University (Permit No: 2011-0039). All experiments were performed in accordance with the approved guidelines. Every effort was made to minimize the suffering of mice.

Whole-body and ex vivo organ fluorescence molecular imaging (FMI)

Whole-animal HFn biodistribution was visualized in gastric tumor xenograft models (SGC-7901 and BGC-823) using a small-animal imaging system (Perkin Elmer Inc.). The mice were anesthetized and injected the IRDye800CW-HFn probe or free IRDye800CW as control, and small-animal imaging was carried out at 0, 4, 6, 12, 24 and 48 h postinjection. After the whole-body fluorescence imaging, the major organs of mice were dissected to

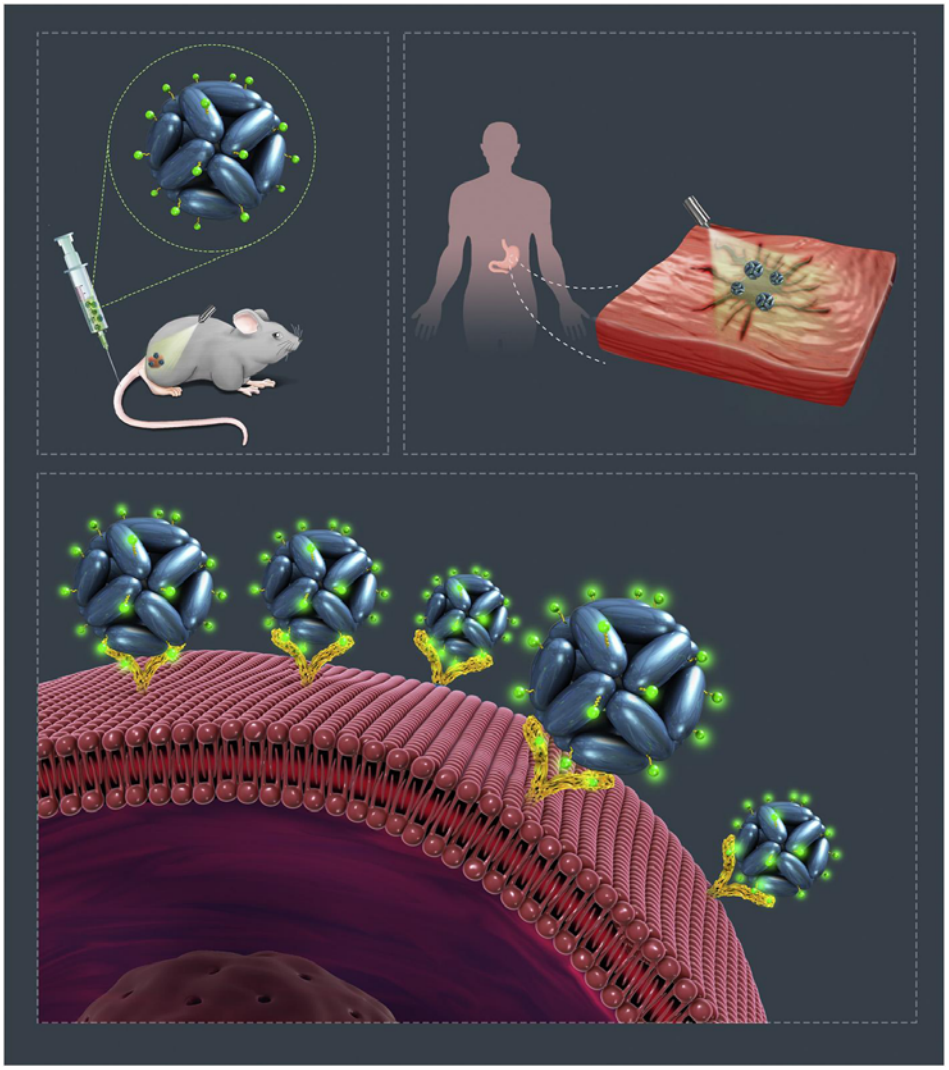

Figure 1. Schematic representation of *in vivo* and *ex vivo* endoscopic molecular imaging of gastric cancers. Targeted imaging of fluorescently labeled HFn is combined with clinical-grade CLE imaging to improve EGC detection. The targeted imaging was validated through both *in vivo* examination of tumor-bearing mice and imaging of excised human EGC specimens.

examine the signal distribution. Imaging was analyzed using IVIS Living Imaging 3.0 software (Perkin Elmer Inc.).

In vivo CLE imaging

In vivo CLE was performed on the two mouse models of human gastric cancer using a probe-based CLE (pCLE) system (Cellvizio® Mauna Kea Technologies), with excitation at 488 nm and emission at 505-585 nm; the imaging was performed on the mice (3/group) 24 h after FITC-HFn injection. After mice were anesthetized, the tumors were exposed, and the confocal probe was positioned on the tumor surface and the signal was scanned. The tumor tissues were processed for histology after the *in vivo* imaging.

Human study

The study protocol was approved by the ethics committee of Peking University Third Hospital, Beijing, China and was conducted in accordance with the Declaration of Helsinki. Written individual informed consent was obtained from the study participants prior to the enrollment of study. Resected human gastric cancer (n = 22) samples and noncancerous tissues (n = 22) from the same patients were rinsed in PBS to remove debris and incubated with FITC-HFn (1 μM) for 30 min at room temperature in the dark. The tissues were then washed with PBS and examined under fluorescence stereomicroscope (Leica, M205 FA, Germany) using the GFP setting (ex 440/470 nm, em 525/550 nm).

The pCLE system was used for CLE imaging of tissue-bound FITC-HFn in the gastric tissue samples, and the obtained images were analyzed semi-quantitatively. The histopathological diagnoses were made by an experienced gastrointestinal pathologist blinded to the results of endomicroscopic observation.

Histological examination

Histopathological evaluation and immunohistochemistry (IHC) analyses were performed on all specimens. Tissue specimens were fixed in 10% formalin, and embedded in paraffin for serial sections at 4-μm intervals. Hematoxylin and

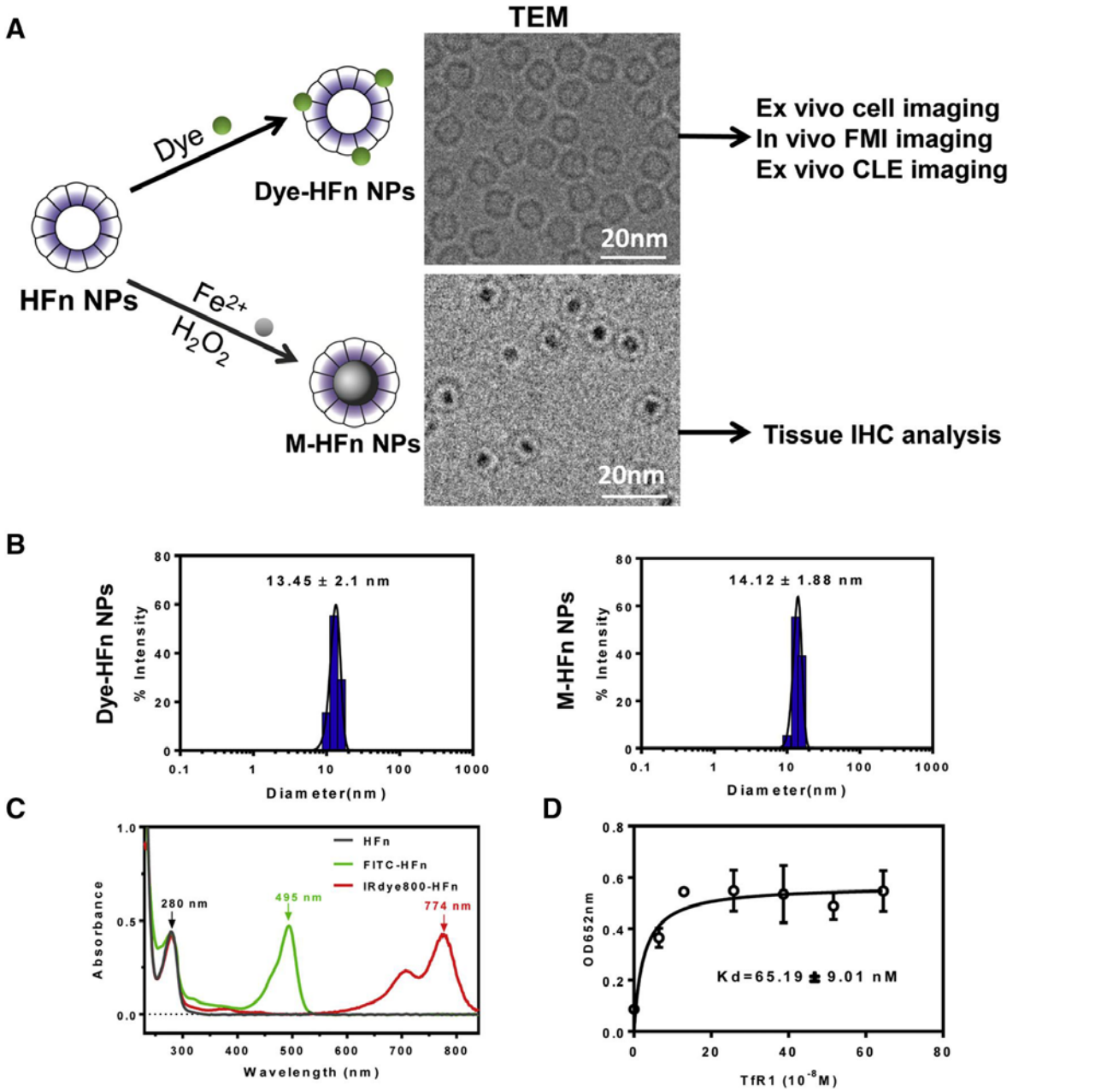

Figure 2. Characterization of HFn-based nanoprobes for CLE and IHC analysis. **(A)** Schematic of dye-HFn nanoprobes for CLE imaging and M-HFn nanoprobes for IHC analysis. The cryo-TEM images show the intact protein-cage structure of dye-HFn and M-HFn. **(B)** DLS analysis of the size distribution of dye-HFn and M-HFn nanoprobes. **(C)** UV–vis spectroscopy analysis of HFn, FITC-HFn, and IRDye800CW-HFn nanoprobes. Arrows: characteristic absorption peaks of the protein, FITC, and IRDye800CW. **(D)** Analysis of HFn nanoprobe binding to TfR1; the binding affinity (equilibrium dissociation constant, Kd) was calculated.

eosin (H&E) staining was performed for the histopathological analyses. The M-HFn-based IHC for EGC tissues was performed as in our previous report.[14] EGC tissues were stained with FITC-HFn as described in previous report.[14]

Statistical analysis

For the endoscopic images of human specimens, FITC-HFn-specific fluorescence intensity was graded as negative (0), weak (+), moderate (++), or strong (+++). This semi-quantitative grading was applied in order to match the *in vivo* staining with scoring in IHC and thereby provide a scale that is clinical transferable. Two investigators, who were blinded to the patients' clinical data and IHC results, ranked CLE images independently. The statistical software GraphPad Prism (v5.0) was utilized for the analysis of the results. The two-sided Fisher exact probability test was used to determine the statistical significance of the differences in fluorescence signal between neoplastic and non-neoplastic human tissue samples. The specific endomicroscopic signal was the outcome variable. κ-correlation was used to compare FITC-HFn-specific staining in CLE *versus* IHC in tissues of the same patients. $P \leq 0.05$ was considered statistically significant.

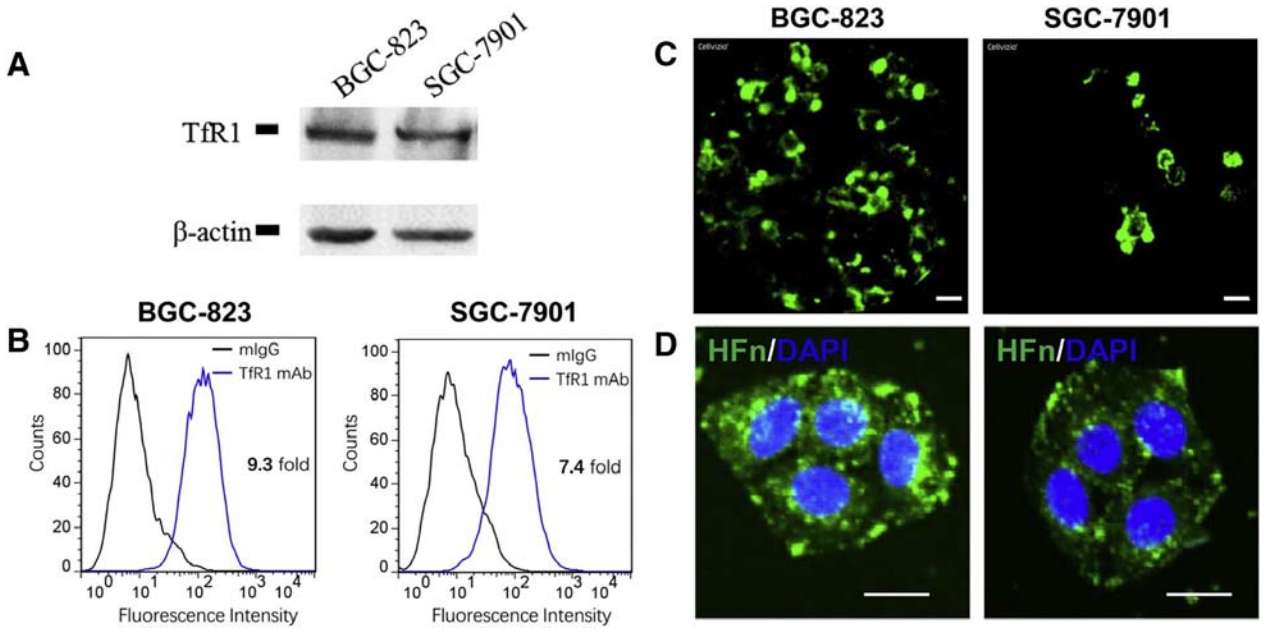

Figure 3. Characterization of TfR1 expression in gastric tumor cells and HFn staining *ex vivo*. **(A)** Western blotting analysis of TfR1 expression in BGC-823 and SGC-7901 gastric tumor cells. **(B)** FACS analysis of BGC-823 and SGC-7901 tumor cells stained with anti-TfR1 and control antibodies. **(C)** *In vitro* CLE imaging of TfR1 expression on BGC-823 and SGC-7901 cells labeled with FITC-HFn. **(D)** Confocal imaging of TfR1-specific fluorescent staining by FITC-HFn, which agrees with the CLE results. Nuclei were stained with DAPI (blue). Scale bar: CLE, 20 μm; fluorescence, 20 μm.

Results

Generation and characterization of the fluorescent HFn binding probe

By exploiting the unique protein nanocage architecture of human HFn, we labeled the protein shell with dye for *in vivo* FMI and *ex vivo* CLE imaging; or we bio-mimetically synthesized highly crystalline iron oxide nanoparticles within the interior cavity of HFn to produce M-HFn for tissue IHC imaging (Figure 2, *A*). The human HFn nanoparticles were recombinantly expressed in *E. coli* and purified as previously reported.[14,17] The HFn nanocage was used as a nanoreactor and the M-HFn nanoparticles were synthesized as previously reported.[14] The dye-HFn and M-HFn nanoprobes were analyzed using cryo-transmission electron microscopy (cryo-TEM); the protein shells of both nanoprobes presented a well-defined morphology and were monodisperse in size (Figure 2, *A*). Uniformly distributed iron oxide nanoparticles were synthesized within the cavity of the HFn nanocages in M-HFn. The size distributions of dye-HFn and M-HFn nanoprobes were determined using Dynamic Light Scattering (DLS); the median diameters were 13.45 ± 2.1 and 14.12 ± 1.88 nm, respectively (Figure 2, *B*). Moreover, UV–vis spectroscopy analysis of dye-HFn nanoprobes confirmed the effective conjugation of FITC and IRDye800CW on the protein shell (Figure 2, *C*). Lastly, the binding affinity of HFn nanoprobes for TfR1 was measured to be 65.19 ± 9.01 nM (Figure 2, *D*), which agrees with the data in our previous work.[14,17]

TfR1 expression by tumor cell lines

TfR1 expression was first characterized *in vitro*. Western blotting results showed the general expression of TfR1 in BGC-823 and SGC-7901 human gastric tumor cell lines (Figure 3, *A*). The TfR1 was weakly expressed in the normal human gastric epithelial cell line GES-1, and there was no expression in the TfR1-negative cell line MX-1 (Figure S1). FACS analysis further confirmed the expression of TfR1 on BGC-823 and SGC-7901 cells; the values obtained with anti-TfR1 were ~9.3- and ~7.4-fold higher than those with IgG control (Figure 3, *B*).

In another set of assays, *in vitro* CLE was performed on BGC-823 and SGC-7901 tumor cells stained with FITC-HFn. The imaging enabled TfR1 visualization in the unfixed tumor cell cultures, in which FITC-HFn showed membranous and cytoplasmic staining patterns (Figure 3, *C*). Notably, these CLE patterns were paralleled and confirmed by the specific fluorescent staining of TfR1 in BGC-823 and SGC-7901 tumor cells by FITC-HFn (Figure 3, *D*). Moreover, to confirm the specific uptake of HFn mediated by the TfR1, the blocking experiment was also performed. The flow cytometry result showed that the mean fluorescence intensity (MFI) was high after incubation with FITC-HFn, but the MFI was significantly decreased after blocking with 100-fold un-labeled HFn in the TfR1 positive BGC-823 gastric cancer cells. For the TfR1 negative MX-1 cells, the MFI was low after incubation with FITC-HFn, and there was no difference after the un-labeled HFn blocking (Figure S1).

Macroscopic fluorescence detection of TfR1 in human gastric tumor xenografts

We used macroscopic whole-body fluorescence detection to dynamically examine the biodistribution and tumor-targeting efficacy of HFn labeled with near-infrared dye (IRDye800CW-HFn) in mice harboring BGC-823 (Figure 4, *A*) and SGC-7901 (Figure 4, *B*) human gastric tumors. The free IRDye800CW was

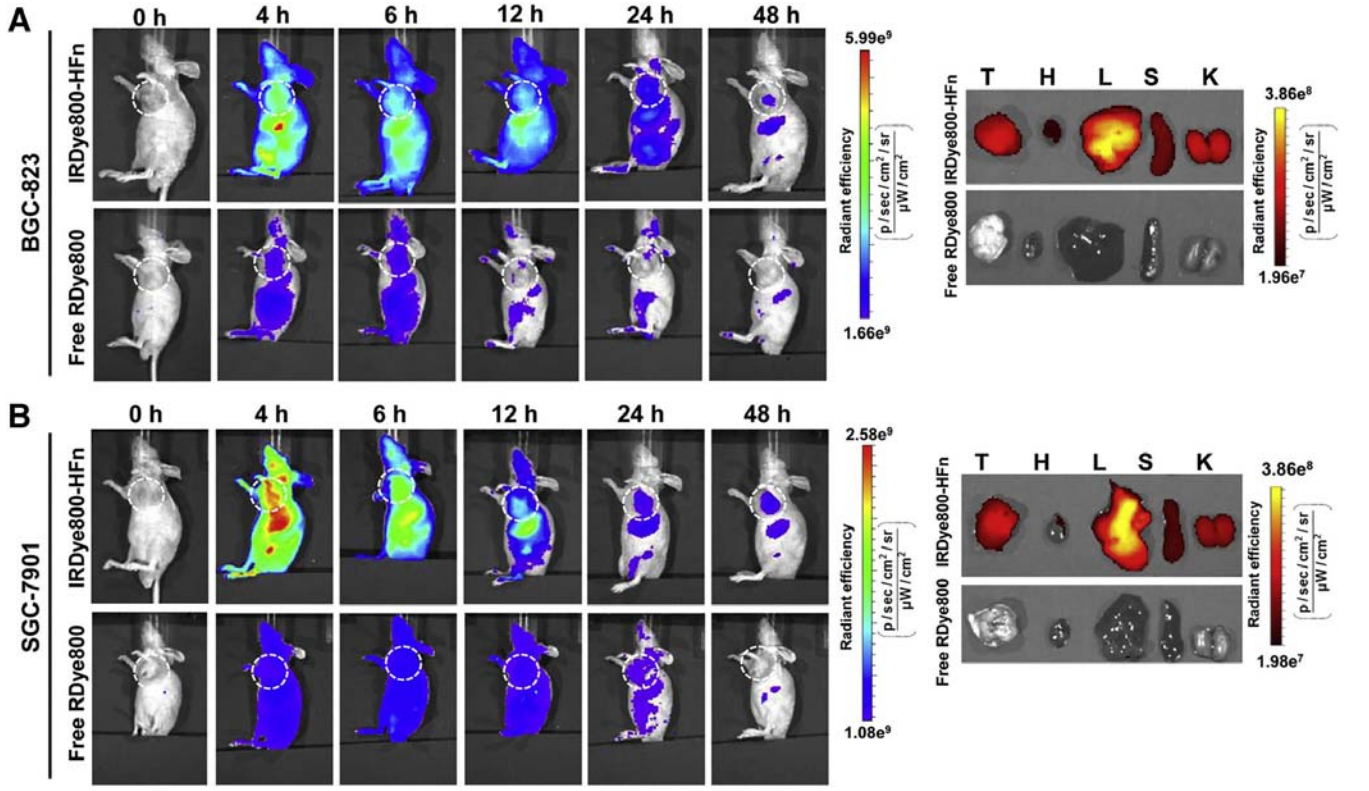

Figure 4. *In vivo* and *ex vivo* fluorescence imaging of IRDye800CW-HFn and free IRDye800CW. Specific *in vivo* fluorescence signals were observed in mice harboring BGC-823 **(A)** and SGC-7901 **(B)** tumors during 48 h of observation after tail-vein injection of IRDye800CW-HFn. *Ex vivo* FMI of tumors and key organs was performed after *in vivo* observation. Mice injected with free IRDye800CW exhibited nonspecific whole-body distribution without enrichment in BGC-823 and SGC-7901 tumors. T, tumor; H, heart; L, liver; S, spleen; K, kidney.

used as control. Both tumor models showed increased HFn-targeted imaging and specific fluorescence signals in the tumors 4 h after tail-vein injection of IRDye800CW-HFn and the signals were still detectable at 48 h after HFn administration, whereas nonspecific distribution of fluorescence signal was detected at the tumor sites in mice injected with free IRDye800CW. The HFn signal was also detected in the liver and kidney, which are the major organs that ferritin nanoparticles are metabolized.[17] After 48 h *in vivo* observation, the tumors and major organs were dissected out and subjected to *ex vivo* fluorescence imaging, and the results agreed well with the *in vivo* observation.

To further confirm the specific HFn uptake *in vivo*, the FMI was also performed on the TfR1-positive BGC-823 tumor xenografts and TfR1-negative MX-1 tumor xenografts after injection with IRDye800CW-HFn. The FMI data showed that there was specific uptake of HFn-IRDye800CW in the BGC-823 tumor xenografts due to the active targeting to the TfR1 in the tumor region, but only weak uptake of HFn-IRDye800CW in the TfR1-negative MX-1 tumor xenografts due to the passively enhanced permeability and retention (EPR) effect of the nanoparticle (Figure S2). The fluorescence imaging of tumor indicated TfR1-specific *in vivo* tumor targeting by fluorescently labeled HFn.

TfR1-targeted imaging in human gastric tumor xenografts

TfR1-targeted CLE imaging was next performed using SGC-7901 and BGC-823 tumor xenografts. 24 h after FITC-HFn injection, the fluorescence signals were detected in the gastric tumor xenografts using CLE, which exhibited TfR1 expression in SGC-7901 and BGC-823 tumors (Figure 5, *A* and *E*). Moreover, *ex vivo* bench-top fluorescence-microscopy imaging (Figure 5, *B* and *F*) and M-HFn IHC staining (Figure 5, *C* and *G*) of paraffin-embedded sections of the tumor xenografts yielded results that were similar to the *in vivo* endomicroscopic findings, and these observations were also confirmed through H&E staining (Figure 5, *D* and *H*).

HFn binding to human EGC tissues ex vivo

Specific binding of FITC-HFn to EGCs was further confirmed by performing CLE *ex vivo* on endoscopic specimens of EGC patients. Table 1 shows the patient characteristics and final pathological diagnoses. The biopsies were histopathologically analyzed by a pathologist who was blinded to the imaging results. To verify that the fluorescence detected on tumors was due to the specific binding of FITC-HFn, the fresh specimens were first incubated with 2% BSA blocking buffer and imaged using CLE, after which they were incubated with FITC-HFn and then imaged again. No signal was detected on either normal or diseased lesions after BSA incubation, but after the subsequent incubation with FITC-HFn, drastically higher fluorescence was detected on cancerous lesions than on noncancerous tissues. Representative frames from confocal videos of normal and diseased lesions in each specimen, together with the

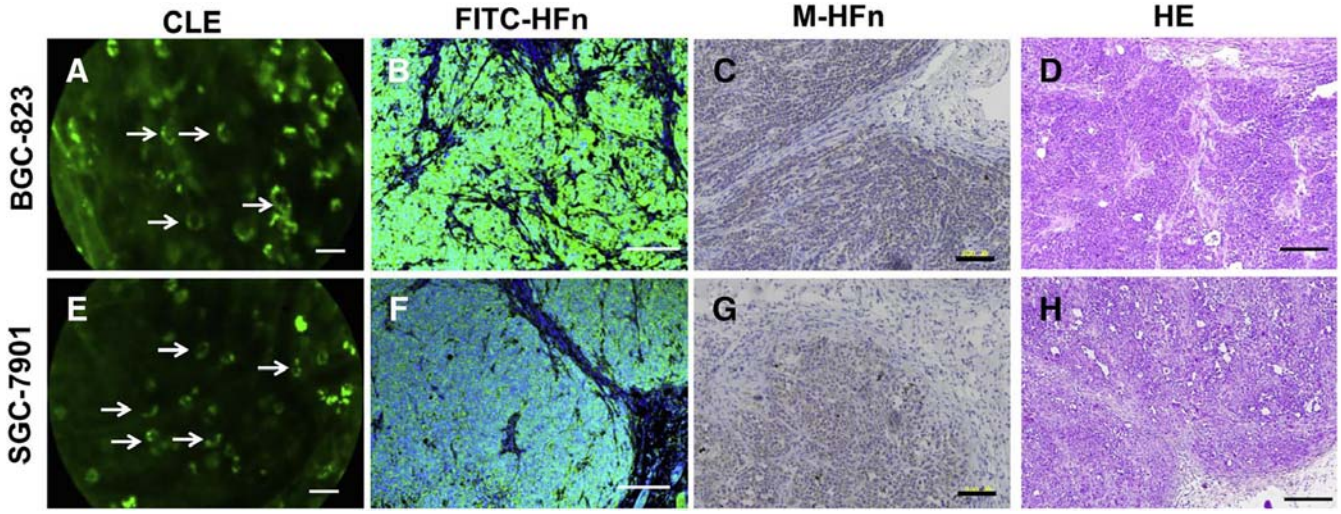

Figure 5. *In vivo* microscopic imaging of human gastric tumor xenografts using CLE. **(A, E)** *In vivo* CLE of gastric tumor xenografts after tail vein injection of FITC-HFn, and arrows indicated the typical positive cells. **(B, F)** *Ex vivo* bench-top fluorescence microscopy performed with FITC-HFn staining and nuclear counterstaining (DAPI), and **(C, G)** M-HFn IHC staining of paraffin sections. **(D, H)** H&E staining of tumor specimens correlated well with the aforementioned observations. Scale bar: CLE, 20 μm; fluorescence, IHC, and H&E staining, 200 μm.

Table 1
Clinicopathological data of patients with gastric carcinomas examined using CLE.

Patients, n	22
Sex, male/female, n	16//6
Age, mean (range),years	67(53-84)
Gastric carcinoma, n	22
Histological differentiation, n	
Poorly differentiated	3
Moderately differentiated	8
Well differentiated	11

corresponding histopathology, are shown in Figure 6. The CLE results showed that a specific TfR1-positive fluorescence signal was present in the neoplastic regions (Figure 6, *A*). The imaging revealed the membranous and cytoplasmic distribution of TfR1 in cancer cells, which agrees with the *in vitro* observation (Figure 6, *B*, white arrows). No obvious fluorescence signal was detected in non-neoplastic regions (Figure 6, *C*). To validate the CLE results, IHC, fluorescence staining, and histological analyses were performed on the tissue sections. The IHC and fluorescence staining revealed specific HFn expression in neoplastic regions (Figure 6, *D-F*) as compared with that in noncancerous regions (Figure 6, *G-I*). To quantify HFn-positive signals in confocal videos, mean fluorescence intensity was determined as an average from all frames in each confocal video. All specimens containing EGCs showed a specific signal after FITC-HFn staining (22/22 lesions), whereas noncancerous tissues exhibited no specific fluorescence (0) (21/22) or weak fluorescence (+) (1/22). The result of a nonparametric test showed a significant difference between neoplastic and non-neoplastic tissues ($P < 0.0001$, chi-square test) (Figure 6, *J*).

Correlation of TfR1 expression level with EGC differentiation degree

Next, we further analyzed the CLE images of FITC-HFn staining in human EGC specimens exhibiting different differentiation degrees (Table 2). HFn fluorescence intensity varied from weak to strong (+ to +++) in 22 neoplastic tissues, which correlated with the differentiation degrees scored as "well," "moderate," and "poor" (Figure 7). The HFn fluorescence signal was weak (+) in well-differentiated neoplasias (Figure 7, *A*), modest (++) in moderately differentiated neoplasias (Figure 7, *B*), and strong (+++) in poorly differentiated neoplasias (Figure 7, *C*). We also performed fluorescence staining (Figure 7, *D-F*) and IHC analysis (Figure 7, *G-I*) on the target tissue specimens, which revealed expression patterns similar to those obtained with *ex vivo* CLE. All of the aforementioned findings were confirmed through H&E staining (Figure 7, *J-L*). The CLE fluorescence ratio of cancerous to noncancerous regions between well and poorly differentiated EGCs was compared, and data showed that it was around 1.8-fold higher for the fluorescence between moderately differentiated to well differentiated tumors, and it was around 1.73-fold higher for the fluorescence between poorly differentiated to moderately differentiated tumors (Figure 7, *M*). Moreover, the κ-coefficient (0.8023) showed a close agreement between endomicroscopic HFn fluorescence signals and IHC results.

FITC-HFn identifies EGC margins

The differentiation between tumor and adjacent nontumorous tissues can be enhanced through fluorescently labeled cancer-specific molecular-imaging agents. Therefore, considerable interest exists in developing molecular-imaging agents that augment tumor visualization. Here, the application of fluorescently labeled HFn as a potential imaging agent for identifying EGC margins was examined using both stereomicroscopy and CLE imaging, as described using the following representative example. In the white-light image, a tumor-lesion area (Figure 8, *A*) was confirmed through histological analysis (shown as regions ① and ② in Figure 8, *B*). After blocking with 2% BSA, FITC-HFn (Figure 8, *C*) was topically applied onto the tumor specimen (Figure 8, *D* and *G*). The staining was initially examined using

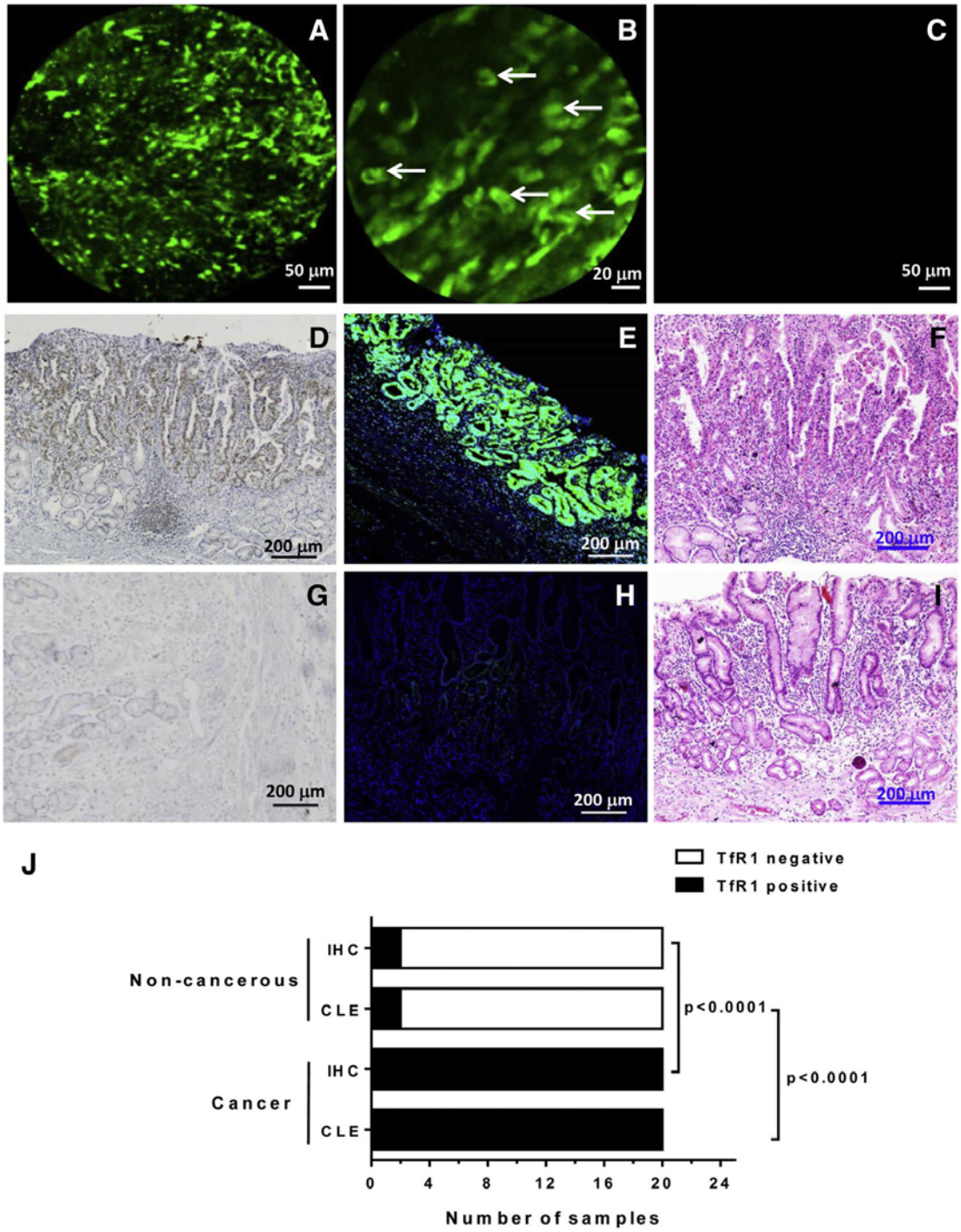

Figure 6. *Ex vivo* validation of the specific binding of HFn nanoprobes to EGCs. Tissue samples from neoplastic lesions were incubated in FITC-HFn solution to mimic topical application during CLE. In CLE, a specific signal was detected in cancerous lesions, and high-magnification imaging showed strong membranous and cytoplasmic staining **(A-B**, arrows**)** as compared with that in noncancerous regions **(C)**. IHC and fluorescence staining revealed specific TfR1 expression, and histopathological analysis confirmed malignancy **(D-F)**. Noncancerous tissues did not exhibit TfR1 staining **(G-I). (J)** TfR1-specific staining was significantly different (as per chi-square tests) between tumorous and nontumorous tissues in CLE and also with the "gold standard" of IHC.

stereomicroscopy, which provides macroscopic images of tissue specimens. The result showed that no detectable signal (autofluorescence signal) was present after BSA blocking (Figure 8, *E* and *H*); by contrast, fluorescence was specifically detected in the tumorous regions ① and ② but not in the adjacent normal regions after FITC-HFn staining (Figure 8, *F* and *I*). The tumor margins are indicated in the images by white dashed lines, and the yellow lines include the entire tissue specimen. The tissue specimen was further examined using CLE, which revealed specific HFn staining in the cancerous region with membranous and cytoplasmic distribution of TfR1 in cancer cells (Figure 8, *J and K*), but no staining in the

Table 2
CLE results on different differentiation degrees of EGCs.

H&E	CLE				Total
	−	+	++	+++	
Normal	21	1	0	0	22
Well differentiated	0	7	4	0	11
Moderately differentiated	0	0	5	3	8
Poorly differentiated	0	0	0	3	3
Total					44

adjacent nontumorous region (Figure 8, *L*). Furthermore, *ex vivo* IHC and fluorescence staining of the same targeted tumor specimen was performed; in both cases, the results demonstrated specific HFn staining of the cancerous region (indicated by red dashed lines in Figure 8, *M-N*) but no staining in the surrounding noncancerous mucosa, and this was subsequently confirmed through H&E staining of the same biopsy specimen (Figure 8, *O*).

FITC-HFn biocompatibility and safety evaluation in animals

Biocompatibility of fluorescently labeled HFn is evaluated using the whole-blood analysis. The data revealed that the total amounts and percentages of white blood cells, lymphocytes, granulocytes, and monocytes were all in the normal range in the FITC-HFn-treated group as control group (Figure S3).

Discussion

Here, we provide first evidence that *in vivo* endoscopic molecular imaging of human EGCs is specific when fluorescently labeled HFn is used. This CLE approach successfully enables specific and safe *in vivo* visualization of TfR1 expression in tumor cells in rodent tumor xenograft models. The preliminary data on resected human tissue specimens of EGCs provided enhanced signal intensity and adequate contrast for CLE imaging after topical application of fluorescently labeled HFn. Moreover, macroscopic fluorescence imaging through stereomicroscopy identified a clear tumor margin featuring a marked fluorescence-signal contrast in the human tissue specimens. Our approach exemplifies a future combination of macroscopic imaging for detection of suspected lesions and CLE for immediate characterization according to the molecular characters.

Currently, the use of antibodies and peptides forms a biological basis for image contrast and provides sufficient image contrast for *in vivo* tumor detection.[18,19] Our study confirmed TfR1 is a promising biomarker for gastric cancers. An intriguing finding reported that TfR1 is a receptor for HFn.[10] However, current HFn-based tumor diagnoses still rely on targeting ligand modification to achieve tumor recognition.[20–25] These modifications destroy the natural tumor-targeting property of human HFn, increase the immunogenicity, and decrease the yield. In this work, we developed fluorescently labeled HFn as a novel CLE nanoprobe for EGC diagnosis that combines several advantages essential for clinical translation of nanomaterials: (a) Excellent tumor recognition: Without ligand modification, HFn specifically recognizes tumor cells through TfR1-mediated tumor targeting. Moreover, the preferential incorporation of HFn by TfR1-positive cells in a threshold-dependent manner results in the specific identification of tumor cells.[15] (b) Low biotoxicity: HFn is naturally expressed in humans, and do not activate inflammatory or immunological responses.[11] (c) High labeling/loading efficiency: Enrichment of amino acid residues on the surface of HFn enables high-efficiency dye labeling.[26] (d) Efficient production: HFn is manufactured using robust and reproducible procedures. Thus, HFn represents an optimal candidate for clinical CLE detection of EGCs.

Our hypothesis is supported by these findings: Gastric tumor xenografts were specifically imaged after systemic application of fluorescently labeled HFn using macroscopic whole-body fluorescence-imaging device and microscopic CLE imaging; Targeted imaging was demonstrated on resected human EGCs, and the data showed 100% sensitivity and 90% specificity with the use of IHC, the same result as CLE. Moreover, a strong correlation was found between the semi-quantitative grading standard of CLE imaging and the IHC results, and positive IHC results were found in all cancerous tissues and were well correlated and in a statistically significant manner with the level of tumor differentiation.

Accurate delineation of tumor margins is essential for achieving high cure rates. Endoscopic resection is the standard therapy for EGC. Recently, CLE has been applied for *in vivo* microscopic diagnosis of gastric cancer, and the technology has been demonstrated to be useful for the detection of gastric lesions.[27–29] Our results have provided evidence that FITC-HFn combined with CLE imaging provides high contrast between cancerous and adjacent normal tissues, which is helpful for identifying EGC margins and endoscopic dissection. As a readily accessible hollow organ, the gastro-intestines offer a well-established route for topical administration of pharmacological agents, and topical administration allows high concentrations of imaging contrast agents to be delivered directly to the suspected mucosa and thus minimizes potential systemic toxicity of imaging agents.

This study's limitations are the following. First, molecular imaging of FITC-HFn after topical administration of the probe in a local region of interest resulted in the fluorescence signal being strongest at the tumor surface (depth $\leq$ 50 μm), and because of the limited penetration depth of the endomicroscopy, the expression status in the entire tumor is not demonstrated. However, this drawback can be overcome using the next generation of confocal systems for near-infrared probes. Second, the patient number in our study was limited. Thus, future investigations will be conducted to confirm the current findings and correlate the tumor-progression features with *in vivo* molecular imaging in a larger study cohort.

In conclusion, this study demonstrates that EGCs are detected by using CLE molecular imaging with HFn-based

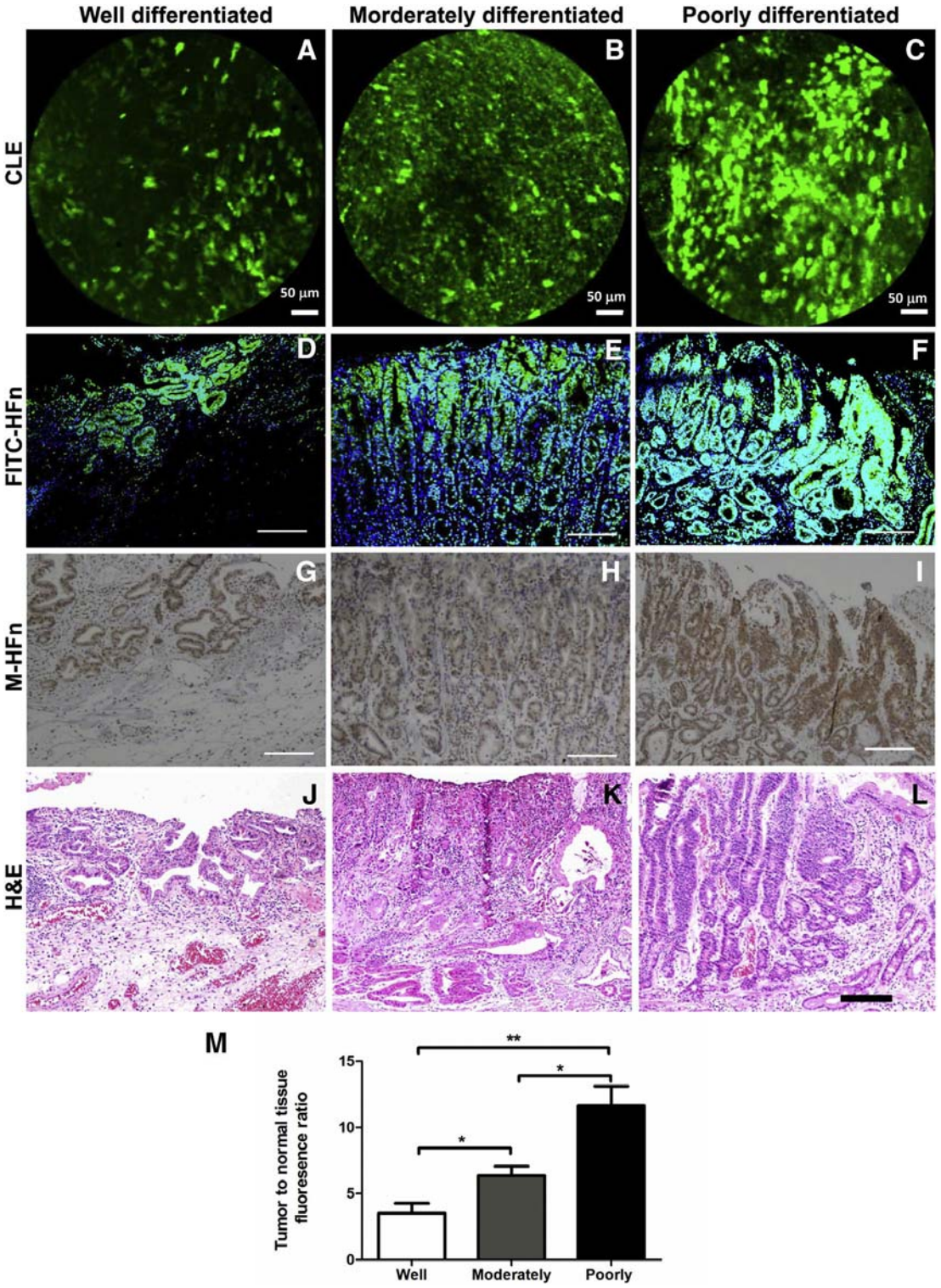

Figure 7. Molecular imaging of fluorescently labeled HFn in EGCs of distinct differentiation degrees. Semi-quantitative evaluation of endomicroscopic images and immunohistopathology of human specimens. **(A-C)** Specific fluorescence signals in CLE images were graded as weak, moderate, and strong (+ to +++). Corresponding fluorescent labeling with FITC-HFn **(D-F)** and M-HFn IHC staining **(G-I)** revealed TfR1 expression patterns. H&E staining confirmed the different degrees of EGC differentiation **(J-L)**. The CLE fluorescence ratio of cancerous to noncancerous region between well and poorly differentiated EGCs **(M)**. IHC, H&E, fluorescence staining: scale bar = 200 μm.

nanoprobes in human gastric tumor xenograft models and human tissues. In further clinical application, this approach will be optimally combined, for example, with the use of a high-resolution macroscopic fluorescence-imaging device. The combined approach would offer a state-of-the-art technique for macroscopic detection and concurrent CLE imaging for

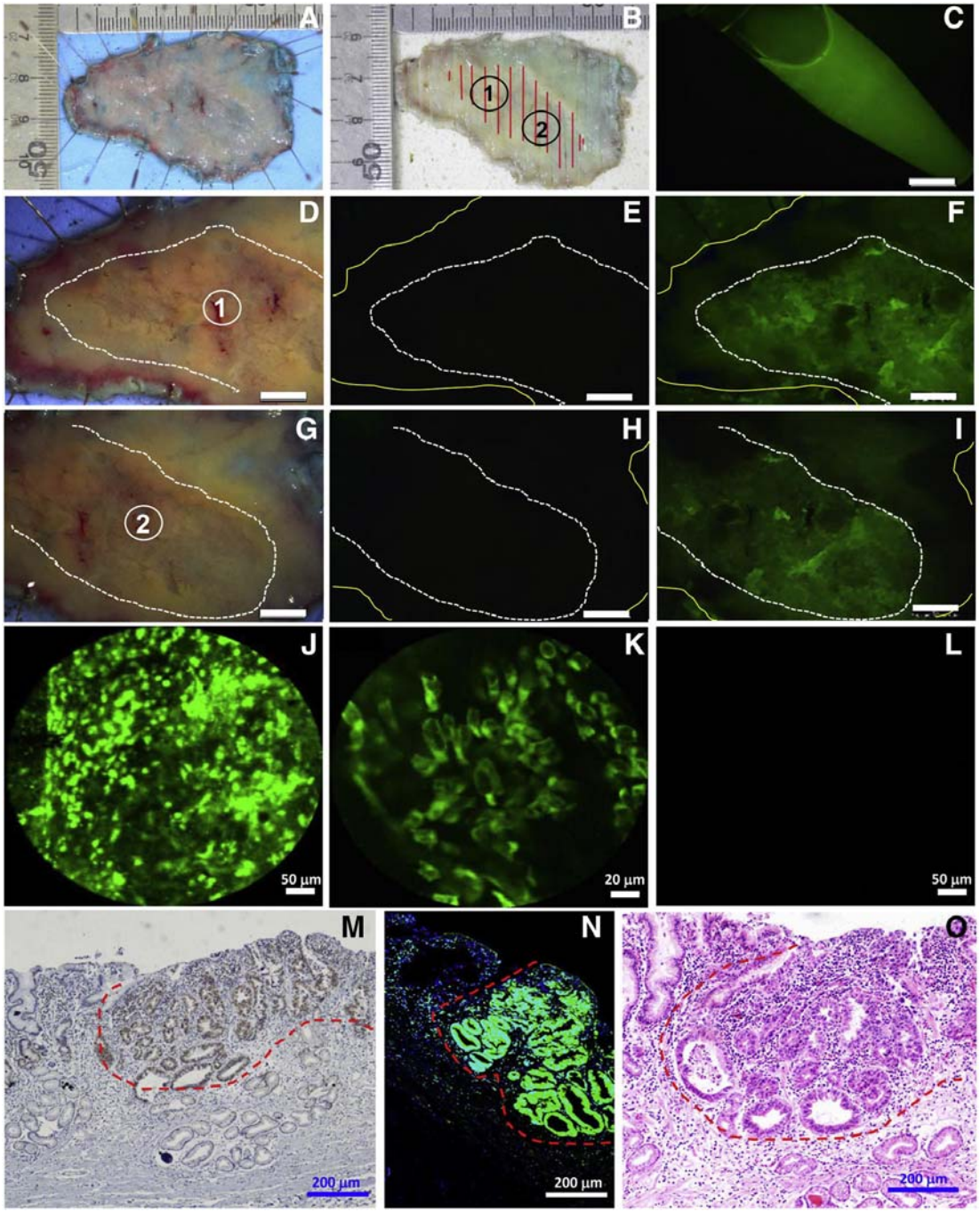

Figure 8. FITC-HFn identifies EGC margins. In the white-light image, a tumor-lesion area **(A)** was confirmed through histological analysis; the area is shown as regions ① and ② **(B)**. The FITC-HFn probe **(C)** was topically applied onto the tumor specimen **(D** and **G)** for staining after blocking with 2% BSA. Stereomicroscopy imaging revealed no detectable signal after BSA blocking **(E** and **H)**; however, after FITC-HFn staining, specific fluorescence was detected in the tumorous regions ① and ② but not in the adjacent normal regions **(F** and **I)**. White dashed lines: tumor margins; yellow lines: entire tissue specimen. In CLE imaging, a specific signal was detected in cancerous lesions, and high-magnification imaging showed strong membranous and cytoplasmic staining **(J** and **K)** as compared with that in noncancerous regions **(L)**. The results of the IHC and bench-top fluorescence staining of the targeted tissue were confirmed through H&E staining (**M-O**; red dashed line: diseased area). Scale bar, C-I, 5 mm.

identifying the real-time molecular expression patterns of lesions. Our findings provide the basis for future targeted CLE imaging in accurate clinical diagnosis of gastric cancers using HFn as a nanoprobe.

Acknowledgments

We thank Dr. Xiaojun Huang and Dr. Gang Ji for excellent technical support in cryo-EM imaging at the Transmission EM

Facilities, Center for Biological Imaging, Institute of Biophysics. We thank Bing Jiang (Institute of Biophysics, CAS) for his assistance of protein purification and dye-labeling experiments.

Appendix A. Supplementary data

Supplementary data to this article can be found online at https://doi.org/10.1016/j.nano.2018.07.007.

References

1. Jemal A, Bray F, Center MM, Ferlay J, Ward E, Forman D. Global cancer statistics. *CA Cancer J Clin* 2011;**61**:69-90.
2. Kiesslich R, Goetz M, Neurath MF. Confocal laser endomicroscopy for gastrointestinal diseases. *Gastrointest Endosc Clin N Am* 2008;**18**:451-66.
3. van Dam GM, Themelis G, Crane LM, Harlaar NJ, Pleijhuis RG, Kelder W, et al. Intraoperative tumor-specific fluorescence imaging in ovarian cancer by folate receptor-α targeting: first in-human results. *Nat Med* 2011;**17**:1315-9.
4. Nguyen QT, Tsien RY. Fluorescence-guided surgery with live molecular navigation–a new cutting edge. *Nat Rev Cancer* 2013;**13**:653-62.
5. Foersch S, Kiesslich R, Waldner M, Galle PR, Neurath MF, Goetz M. In vivo molecular imaging of VEGF in gastrointestinal cancer using confocal laser endomicroscopy. *Gastrointest Endosc* 2010;**59**(8):1046-55.
6. Hsiung P, Hardy J, Friedland S, Soetikno R, Du CB, Wu APW, et al. Detection of colonic dysplasia in vivo using a targeted fluorescent septapeptide and confocal microendoscopy. *Nat Med* 2008;**14**:454-8.
7. Pan Y, Volkmer JP, Mach KE, Rouse RV, Liu JJ, Sahoo D, et al. Endoscopic molecular imaging of human bladder cancer using a CD47 antibody. *Sci Transl Med* 2014;**6**:260ra148.
8. Goetz M, Ziebart A, Foersch S, Vieth M, Waldner MJ, Delaney P, et al. In vivo molecular imaging of colorectal cancer with confocal endomicroscopy by targeting epidermal growth factor receptor. *Gastroenterology* 2010;**138**:435-46.
9. Daniels TR, Bernabeu E, Rodríguez JA, Patel S, Kozman M, Chiappetta DA, et al. The transferrin receptor and the targeted delivery of therapeutic agents against cancer. *Biochim Biophys Acta* 1820;**2012**:291-317.
10. L L, CJ F, JC R, EC N, JA L, PJ B, et al. Binding and uptake of H-ferritin are mediated by human transferrin receptor-1. *Proc Natl Acad Sci* 2010;**107**:3505-10.
11. Fan K, Gao L, Yan X. Human ferritin for tumor detection and therapy. *Wiley Interdiscip Rev Nanomed Nanobiotechnol* 1900;**5**:287-98.
12. Harrison PM, Arosio P. The ferritins: molecular properties, iron storage function and cellular regulation. *Biochim Biophys Acta* 1996;**1275**:161-203.
13. Wang Z, Gao H, Zhang Y, Liu G, Niu G, Chen X. Functional ferritin nanoparticles for biomedical applications. *Front Chem Sci Eng* 2017;**11**:633-46.
14. Fan K, Cao C, Pan Y, Lu D, Yang D, Feng J, et al. Magnetoferritin nanoparticles for targeting and visualizing tumour tissues. *Nat Nanotechnol* 2012;**7**:459-64.
15. Sakamoto S, Kawabata H, Masuda T, Uchiyama T, Mizumoto C, Ohmori K, et al. H-ferritin is preferentially incorporated by human erythroid cells through transferrin receptor 1 in a threshold-dependent manner. *PLoS One* 2015;**10**e0139915.
16. Fan K, Jia X, Zhou M, Wang K, Conde J, He J, et al. Ferritin nanocarrier traverses the blood brain barrier and kills glioma. *ACS Nano* 2018.
17. Liang M, Fan K, Zhou M, Duan D, Zheng J, Yang D, et al. H-ferritin-nanocaged doxorubicin nanoparticles specifically target and kill tumors with a single-dose injection. *Proc Natl Acad Sci U S A* 2014;**111**:14900-5.
18. Sturm MB, Joshi BP, Lu S, Piraka C, Khondee S, Elmunzer BJ, et al. Targeted imaging of esophageal neoplasia with a fluorescently labeled peptide: first in-human results. *Sci Transl Med* 2013;**5**:184ra61.
19. Burggraaf J, Kamerling IMC, Gordon PB, Schrier L, Kam MLD, Kales AJ, et al. Detection of colorectal polyps in humans using an intravenously administered fluorescent peptide targeted against c-Met. *Nat Med* 2015;**21**:955-61.
20. Uchida M, Flenniken ML, Allen M, Willits DA, Crowley BE, Brumfield S, et al. Targeting of cancer cells with ferrimagnetic ferritin cage nanoparticles. *J Am Chem Soc* 2006;**128**:16626-33.
21. Li X, Qiu L, Zhu P, Tao X, Imanaka T, Zhao J, et al. Epidermal growth factor–ferritin H-chain protein nanoparticles for tumor active targeting. *Small* 2012;**8**:2505-14.
22. Lin X, Xie J, Niu G, Zhang F, Gao H, Yang M, et al. Chimeric ferritin nanocages for multiple function loading and multimodal imaging. *Nano Lett* 2011;**11**:814-9.
23. Zhen Z, Tang W, Chen H, Lin X, Todd T, Wang G, et al. RGD-modified apoferritin nanoparticles for efficient drug delivery to tumors. *ACS Nano* 2013;**7**:4830-7.
24. Zhen Z, Tang W, Guo C, Chen H, Lin X, Liu G, et al. Ferritin nanocages to encapsulate and deliver photosensitizers for efficient photodynamic therapy against cancer. *ACS Nano* 2013;**7**:6988-96.
25. Zhen Z, Tang W, Chuang YJ, Todd T, Zhang W, Lin X, et al. Tumor vasculature targeted photodynamic therapy for enhanced delivery of nanoparticles. *ACS Nano* 2014;**8**:6004-13.
26. Schoonen L, van Hest JC. Functionalization of protein-based nanocages for drug delivery applications. *Nanoscale* 2014;**6**:7124-41.
27. Kakeji Y, Yamaguchi S, Yoshida D, Tanoue K, Ueda M, Masunari A, et al. Development and assessment of morphologic criteria for diagnosing gastric cancer using confocal endomicroscopy: an *ex vivo* and *in vivo* study. *Endoscopy* 2006;**38**:886-90.
28. Kitabatake S, Niwa Y, Miyahara R, Ohashi A, Matsuura T, Iguchi Y, et al. Confocal endomicroscopy for the diagnosis of gastric cancer *in vivo*. *Endoscopy* 2006;**38**:1110-4.
29. Li WB, Zuo XL, Li CQ, Zuo F, Gu XM, Yu T, et al. Diagnostic value of confocal laser endomicroscopy for gastric superficial cancerous lesions. *Gut* 2011;**60**:299-306.